Article:
Lu, Y., Dewald, N., Koutsodendris, A. et al. (6 more authors) (2020) Sedimentological evidence for pronounced glacial-interglacial climate fluctuations in NE Tibet in the latest Pliocene to early Pleistocene. Paleoceanography and Paleoclimatology, 35 (5). ISSN 2572-4517

https://doi.org/10.1029/2020pa003864

Paleoceanography and Paleoclimatology

RESEARCH ARTICLE
10.1029/2020PA003864

Sedimentological Evidence for Pronounced Glacial-Interglacial Climate Fluctuations in NE Tibet in the Latest Pliocene to Early Pleistocene

Yin Lu[1,2], Nico Dewald[1,3], Andreas Koutsodendris[1], Stefanie Kaboth-Bahr[1,4], Wolfgang Rösler[5], Xiaomin Fang[6,7], Jörg Pross[1], Erwin Appel[5], and Oliver Friedrich[1]

[1]Institute of Earth Sciences, Heidelberg University, Heidelberg, Germany, [2]Now at Geomorphology and Quaternary Geology Research Group, University of Liege, Liege, Belgium, [3]Department of Geography, The University of Sheffield, Sheffield, UK, [4]Institute of Geosciences, University of Potsdam, Potsdam-Golm, Germany, [5]Institute of Geosciences, University of Tübingen, Tübingen, Germany, [6]Key Laboratory of Continental Collision and Plateau Uplift, Institute of Tibetan Plateau Research, Chinese Academy of Sciences, Beijing, China, [7]CAS Center for Excellence in Tibetan Plateau Earth Sciences, Chinese Academy of Sciences, Beijing, China

Key Points:
- Pronounced glacial-interglacial climate fluctuations on the NE Tibetan Plateau during the latest Pliocene and early Pleistocene
- Changes in East Asian Winter Monsoon and the position of the westerlies influenced sediment transport on the NE Tibetan Plateau
- Intensification of Northern Hemisphere glaciation amplified climate fluctuations on the NE Tibetan Plateau

Supporting Information:
- Supporting Information S1
- Figure S1
- Figure S2

Correspondence to:
Y. Lu,
yinlusedimentology@yeah.net
yin.lu@uliege.be

Citation:
Lu, Y., Dewald, N., Koutsodendris, A., Kaboth-Bahr, S., Rösler, W., Fang, X., et al (2020). Sedimentological evidence for pronounced glacial-interglacial climate fluctuations in NE Tibet in the latest Pliocene to early Pleistocene. *Paleoceanography and Paleoclimatology*, *35*, e2020PA003864. https://doi.org/10.1029/2020PA003864

Received 27 JAN 2020
Accepted 4 APR 2020
Accepted article online 14 APR 2020

Abstract The intensification of Northern Hemisphere glaciation (iNHG) and uplift of the Tibetan Plateau have been argued to be among the main drivers of climate change in midlatitude Central Asia during the Pliocene/Pleistocene. While most proxy records that support this hypothesis are from regions outside the Tibetan Plateau (such as from the Chinese Loess Plateau), detailed paleoclimatic information for the plateau itself during that time has yet remained elusive. Here we present a temporally highly resolved (~500 years) sedimentological record from the Qaidam Basin situated on the northeastern Tibetan Plateau that shows pronounced glacial-interglacial climate variability during the interval from 2.7 to 2.1 Ma. Glacial (interglacial) intervals are generally characterized by coarser (finer) grain size, minima (maxima) in organic matter content, and maxima (minima) in carbonate content. Comparison of our results with Earth's orbital parameters and proxy records from the Chinese Loess Plateau suggests that the observed climate fluctuations were mainly driven by changes in the Siberian High/East Asian winter monsoon system as a response to the iNHG. They are further proposed to be enhanced by the topography of the Tibetan Plateau and its impact on the position and intensity of the westerlies.

1. Introduction

The latest Pliocene/early Pleistocene intensification of Northern Hemisphere glaciation (iNHG) marks a decisive step within the Earth's long-term cooling during the Cenozoic (Hill et al., 2017; Ravelo et al., 2004; Zachos et al., 2008; Zhang et al., 2009). In marine records, the iNHG is marked by increasing amplitudes of benthic $\delta^{18}O$ values (Lisiecki & Raymo, 2005) that resulted from high-amplitude climate fluctuations (Ravelo et al., 2004; Bartoli et al., 2006; Sosdian & Rosenthal, 2009; Friedrich et al., 2013; Jakob et al., 2017). The timing when glaciers formed in coastal high-latitude settings of the Northern Hemisphere is thereby marked by the appearance of ice-rafted debris in both North Atlantic and North Pacific sediments from 2.7 Ma onward (De Schepper et al., 2014; Kleiven et al., 2002; Maslin et al., 1998; Shackleton et al., 1984).

For the terrestrial realm, knowledge about the feedbacks between climate change and the iNHG is mainly based on lake sediments (Williams et al., 1997; Pross & Klotz, 2002; An et al., 2011), terrigenous proxy data sets from marine drill cores (Demenocal, 2004; Grant et al., 2017; Naafs et al., 2012), and loess sequences (Ding et al., 2002; Sun et al., 2006, 2010). In these records, the iNHG is marked by high-amplitude fluctuations in temperature- and/or precipitation-related parameters. However, such high-resolution data are yet scarce for the upper Pliocene and lower Pleistocene of the Tibetan Plateau (Cai et al., 2012; Herb et al., 2015; Koutsodendris et al., 2019), although this region represents one of the most sensitive regions to climate change.

Representing the largest continental plateau on Earth, the Tibetan Plateau has a substantial impact on the Earth's climate evolution during the Late Cenozoic (An et al., 2001; Raymo & Ruddiman, 1992; Rea

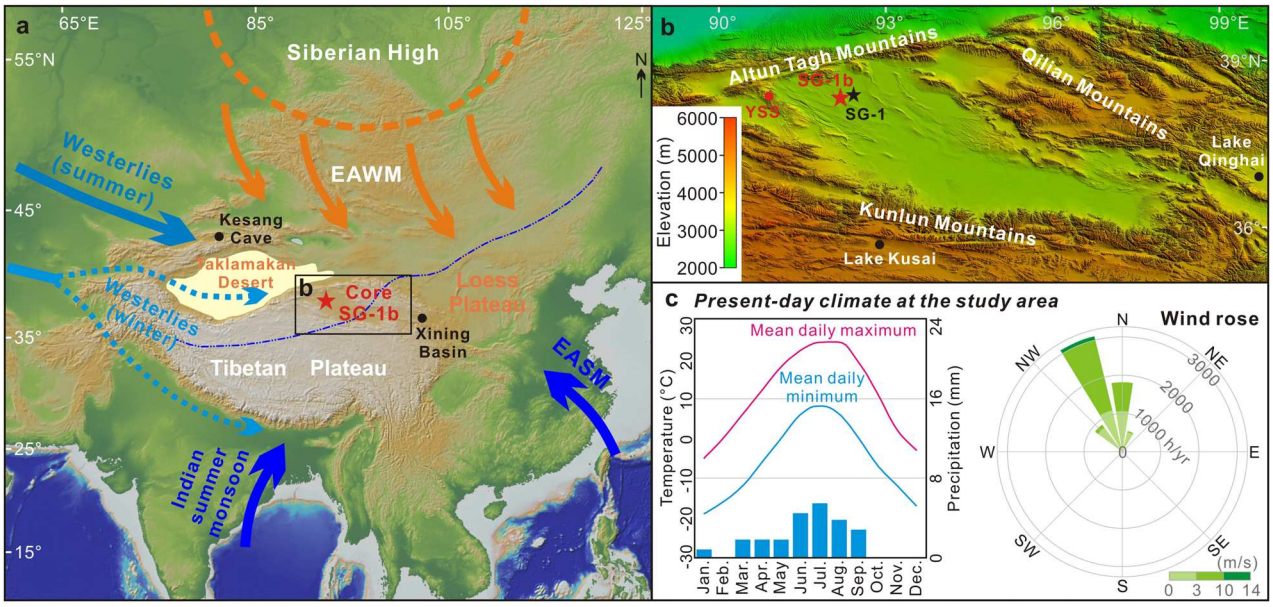

Figure 1. Geological setting and atmospheric circulation pattern of the study region. (a) Atmospheric circulation pattern of the study region; EAWM = East Asian winter monsoon; EASM = East Asian summer monsoon; the dashed blue line indicates the limit of modern Asian summer monsoon influence (Gao et al., 1962). (b) Core location (red star) and topography of the Qaidam Basin and surrounding area. (c) Present-day climate of the study area (adopted from: https://www.meteoblue.com/en/weather/forecast/modelclimate); the meteorological data are simulated based on observed weather data of observational stations in the west and east of the drilling site. The black points and star in panels (a) and (b) indicate localities referred to in the text; YSS, Youshashan, where modern eolian deposits have been collected.

et al., 1998; Ruddiman & Kutzbach, 1989). Previous studies of lacustrine (Herb et al., 2015; Koutsodendris et al., 2018; Liu et al., 2009; Yang et al., 2017) and eolian (Lu et al., 2004; Wang et al., 2015) sedimentary sequences have documented short- and long-term climatic fluctuations on the NE Tibetan Plateau since at least the early Pleistocene. To a varying extent, these fluctuations have been linked to high-northern-latitude glaciations and variations of both the East Asian winter monsoon (EAWM) and the East Asian summer monsoon (EASM). For the latest Pliocene and early Pleistocene, however, information about the feedbacks between iNHG and high-amplitude climate fluctuations in this region is still absent due to the lack of long records with sufficiently high (i.e., centennial to millennial scale) temporal resolution.

Here we present high-resolution (~500 years) grain size, loss on ignition (LOI), and lithology records spanning the time interval ~2.7–2.1 Ma from the western Qaidam Basin, NE Tibetan Plateau. The region is intensely affected by both the EAWM and the westerlies (Herb et al., 2015; Kapp et al., 2011; Wischnewski et al., 2011), representing the dominant climate systems in Central Asia. In addition, recent observations from the northern Qaidam Basin (Li et al., 2015) as well as paleo-records from NE Tibet (Liu et al., 2009) and Xinjiang (Cheng et al., 2012) also suggest an occasional influence of the EASM during the Holocene. Our high-resolution terrestrial record from Core SG-1b therefore can yield a detailed picture of natural climatic variability on the NE Tibetan Plateau across the iNHG. Furthermore, this record enables us to explore the potential interplay between the westerlies, Siberian High/EAWM, and EASM, and how these influenced Central Asian climate across the critical Pliocene/Pleistocene transition.

2. Study Area, Material, and Chronology

2.1. Study Area

Covering an area of ~120,000 km^2, the Qaidam Basin is the largest intermontane basin on the Tibetan Plateau (Figure 1a). It is surrounded by the Qilian Mountains to the north, the Kunlun Mountains to the south, and the Altun Tagh Mountains to the west (Figure 1b). The interior of the basin has a mean elevation of ~2,800 m above sea level, while the surrounding mountains reach up to ~5,000 m, providing a regional source of clastic sediments (Xia et al., 2001; Yin et al., 2008). The basin has formed as a consequence of the still ongoing India-Asia collision and received up to 12-km-thick Cenozoic sediments (Fang et al., 2007;

Xia et al., 2001). In Oligocene times, a large paleolake formed in the western part of the Qaidam Basin (Yang, 1986). The lake expanded in size during the Miocene and underwent dramatic shrinkage during the Pliocene-Pleistocene due to (i) regional uplift in the western part of the basin and subsidence in the eastern part (Fang et al., 2007; Xia et al., 2001; Yin et al., 2008) and (ii) intensification of aridity from ~3.6 Ma onward (Cai et al., 2012; Koutsodendris et al., 2019; Li et al., 2014). The extremely low annual precipitation (mean: <50 mm), very high annual potential evaporation (mean: ~3,000 mm), and strong winds (Qiang et al., 2006) characterize present-day climate in the Qaidam Basin (Figure 1c). In such an inland hyperarid basin, seasonal fluvial input and strong winds are the primary drivers of sedimentation (Kapp et al., 2011; Lu et al., 2015; Pullen et al., 2011; Qiang et al., 2007).

2.2. Material and Chronology

As part of a joint Sino-German project, the 723-m-deep core SG-1b (38°21′9.46″N, 92°16′24.72″E) has been drilled in the western Qaidam Basin (Figure 1b). In this study, we focus on the core interval between ~101 and 56 m, which represents a lacustrine sequence mainly composed of mudstones, siltstones, and evaporites (Lu et al., 2015). Paleomagnetic dating constrains the investigated succession to span from ~2.7 to 2.1 Ma (Zhang et al., 2014). This chronology has been further refined by an astronomical tuning (Kaboth-Bahr et al., 2020). The tuning was established using the ln (Rb/Sr) ratio derived from XRF core scanning since the Rb/Sr ratio has been demonstrated to be highly sensitive to humidity changes (Chen et al., 1999), it is used as a tracer for wet-dry climate alternations at Qaidam Basin. The wet-dry cycles in the core sediments from the Qaidam Basin were subsequently tuned to glacial–interglacial climate variability paced by obliquity during the time interval 3.2–2.1 Ma (Kaboth-Bahr et al., 2020). According to this age model, the study material spans the time interval from ~2.7 to 2.1 Ma.

3. Methods

3.1. Sampling and Facies Description

Samples for LOI and grain size measurements have been collected and measured at 4 cm intervals, providing a temporal resolution of ~500 years based on the astronomically tuned age model for Core SG-1b (Kaboth-Bahr et al., 2020). High-resolution core image scanning has been performed on the undisturbed archive half of Core SG-1b at the Institute of Earth Sciences, Heidelberg University, using an Avaatech fourth generation XRF Scanner equipped with a CCD-Color Line Scan Camera. Basic lithofacies of the studied core interval have been identified and defined based on these high-resolution core images and macroscopic observations.

3.2. LOI

Loss on ignition is a common and widely used method to estimate the organic matter and carbonate contents of lacustrine sediments (Dean, 1974; Heiri et al., 2001). LOI of sediments from Core SG-1b has been performed at the Institute of Earth Sciences, Heidelberg University, following the procedure described in Heiri et al. (2001). Bulk samples were freeze-dried for 24 hr and ~1 g of crushed sediment from each sample has been weighed. Subsequently, the samples were fired at 550 °C (LOI-550 °C) for 4 hr and weighed. The lost weight during burning is then used to estimate the organic matter content of the sample. Following this procedure, the samples were fired at 950 °C (LOI-950 °C) for 2 hr and weighed again to estimate the loss of weight during this second burning step that gives an estimate of the carbonate content of the samples.

3.3. Grain Size

Grain sizes between 0.08 μm and 2 mm have been determined using a laser-particle sizer Fritsch Analysette 22 at the Institute of Earth Sciences, Heidelberg University, following the procedure of Konert and Vandenberghe (1997). Samples were pretreated with 10–15 ml of 30% H_2O_2 to remove organic matter, then with 10–15 ml of 8% HCl to remove carbonates, and finally washed with distilled H_2O. Prior to analysis, the samples were treated with 10 ml of 0.12 mol $Na_4P_2O_7{\cdot}10H_2O$ on an ultrasonic vibrator for 10 min. GRADISTAT Version 6.0 (Blott & Pye, 2001) has been used to calculate the mean grain size of each sample.

Subsequently, the grain size distribution was analyzed using the end-member modeling analysis (EMMA) as included in the R package "EMMA developed" (Dietze et al., 2012). This method is a powerful tool for the unmixing of grain size distributions into significant sediment subpopulations, that is, end members. To

estimate the optimal number of end members required, the coefficients of determination were automatically calculated. The coefficient of determination represents the proportion of the variance of each grain size class that can be reproduced by the approximated data. This proportion is equal to the squared correlation coefficient (R^2) of the input variables.

3.4. SEM

Three silt samples each from the prominent Marine Isotope Stage (MIS) 100 and 96 glacials and the MIS 85 interglacial have been chosen to analyze the morphology and surface texture of quartz grains. To compare the quartz grains from Core SG-1b with modern eolian deposits, one sample from a modern sand dune in Youshashan (western Qaidam Basin) has been collected and analyzed as well. All samples were pretreated with 30% H_2O_2 to remove organic matter, subsequently boiled in 25% HCl to remove carbonates, and finally washed with distilled H_2O. Individual grains of sediments from Core SG-1b have been examined with a ZEISS WITec RISE EVO MA15 using an electron high tension of 30 kV at the Institute of Earth Sciences, Heidelberg University. Grains of modern eolian deposits from Youshashan were examined with a JEOL JSM-IT300 Scanning Electron Microscopy (SEM) using a 12-kV accelerating potential at the Institute of Tibetan Plateau Research, Chinese Academy of Sciences.

3.5. Petrography of Oolit-Bearing Mudstones

Two thin sections from oolite-bearing mudstones layers from core interval of SG-1b were examined with a reflected-light microscope and photographed with a digital camera at the Institute of Earth Sciences, Heidelberg University. Verifying and revealing the nature of the ooids will be important for facies interpretation.

4. Results and Discussion

4.1. Lithofacies and Its Environmental Implication

Seven distinct lithofacies dominate the lacustrine sequence of the study interval (Figure 2). To gain an environmental interpretation, we concentrated on the preserved sedimentary structures, textures, LOI, and grain size distributions of these lithofacies.

Facies I is a mudstone characterized by the presence of dark gray to black, submillimeter-sized laminations. Carbonate content of these mudstones is low (4–11% of LOI-950 °C), while the organic matter content is generally high (11–17% of LOI-550 °C) (Figure 1a). Grain size analyses show that the sediments are mainly composed of clay and fine-silt particles (<16 μm). The occurrence of well-preserved dark gray to black, submillimeter-thick laminations and the high organic matter content imply a stagnant deep-water environment characterized by a lack of bioturbation and an enhanced preservation of organic matter. Investigations in grain size of surface samples from modern lakes across the Tibetan Plateau (Lu et al., 2018), further support the Facies I is deposited in a stagnant central lake zone.

Facies II is characterized by mudstones with a homogeneous texture (Figure 2b), which can be attributed to low-density flow processes. With respect to its carbonate (4–15% of LOI-950 °C) and organic matter (11–15% of LOI-550 °C) content and the observed grain size distribution (<16 μm), this facies shows similar features than Facies I but lacks laminations. Based on a generally fine grain size, high organic matter and low carbonate content, and the well-preserved sedimentary structures of laminae in Facies I, we suggest that Facies I and II are indicative of high lake levels under a relatively humid climate.

Facies III can be separated from Facies I and II by the occurrence of numerous yellowish-gray millimeter-thick silty layers and coarser modes (10.5 μm vs. 4.5 μm; Figures 2a and 2c) of the grain size distribution curves. The thicker brown mud layers of Facies III are proposed to reflect similar depositional processes as Facies II. LOI-950 °C (indicating carbonate content) of these sediments varies between 5% and 18% and is slightly higher than in Facies I and II, while the LOI-550 °C (indicating organic matter content) shows values between 8% and 14%, which are slightly lower than those compared to Facies I and II (Figure 1a). The grain size distributions of Facies III are very similar to typical Quaternary clayey loess from the Chinese Loess Plateau (Sun et al., 2004), which may suggest an increasing input of eolian particles into the lake.

Facies IV is defined by a high content of coarse silt (Figure 2d). This facies shows variations of LOI-550 °C and LOI-950 °C in the range of 7–14% and 5–21%, respectively (Figure 2d). We further separate this facies

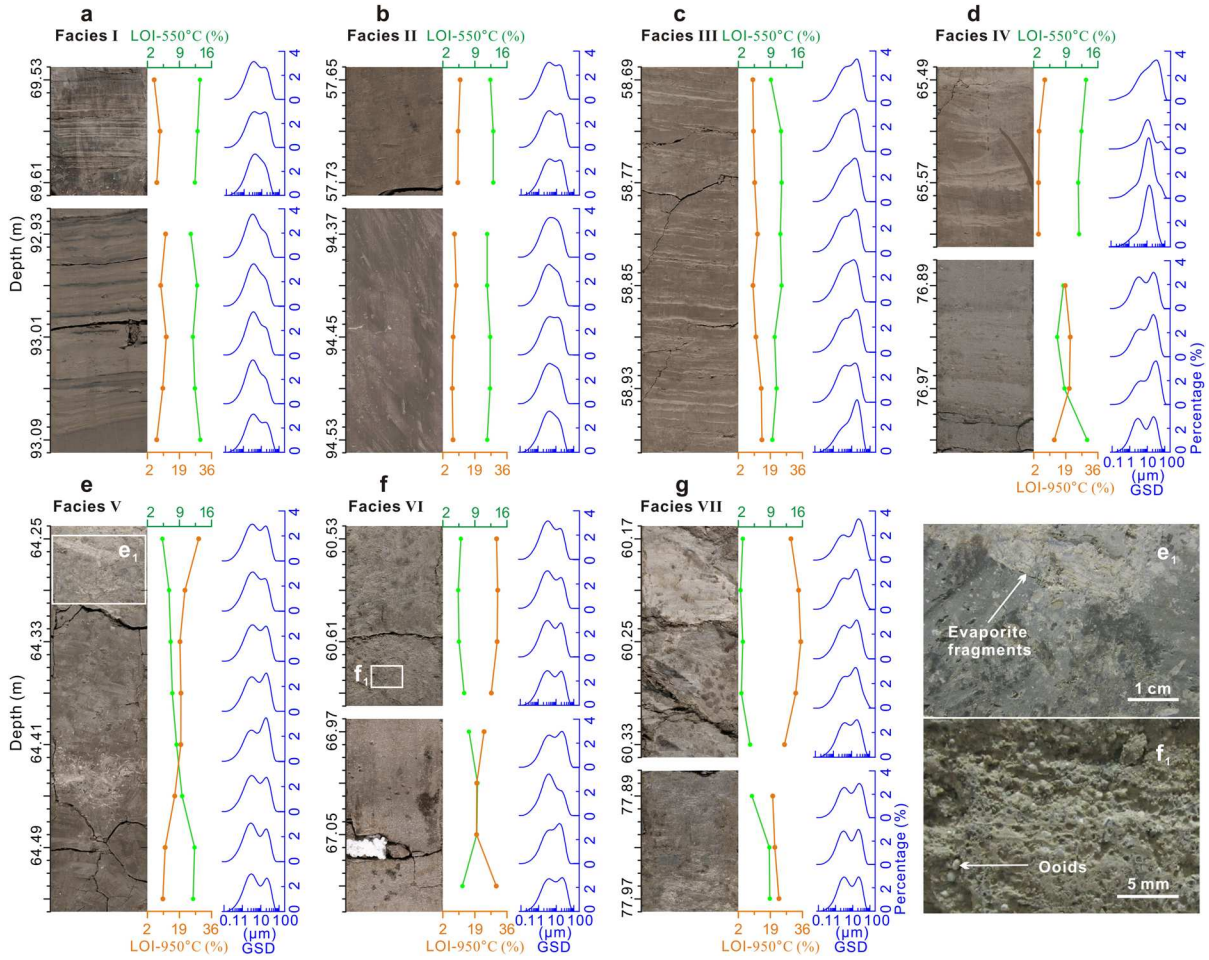

Figure 2. Basic lithofacies in the studied lacustrine sequence of Core SG-1b. (a) Facies I: mud containing submillimeter-sized clayey lamination. (b) Facies II: homogeneous mud. (c) Facies III: mud interbedded by millimeter-thick silty layers. (d) Facies IV: coarse silt layers. (e) Facies V: mud containing evaporitic fragments (see text for process interpretation). (f) Facies VI: mud containing ooids. (g) Facies VII: evaporites containing mud. (e_1) Enlarged image of Figure 2e showing evaporitic fragments in Facies V. (f_1) Enlarged image from Figure 2f showing ooids contained in Facies VI. LOI = loss on ignition; GS = grain-size distribution; diameter of the core is 8 cm. For enlarged images of the cores see Figure S1 in the supporting information.

into two basic types according to their different features of grain size distribution. The first type of these sediments (upper part of Figure 2d) shows a homogeneous texture and similar grain size distributions compared to the typical Quaternary silty loess from the Chinese Loess Plateau (Shang et al., 2018) and modern dust from the Qinghai Lake area, NE Tibetan Plateau (An et al., 2012). This implies an enhanced input of eolian particles, a view which is confirmed by SEM examination on quartz grains (Figure 3c; core depth: 65.53 m). These quartz grains show high sphericity and high roundness, which is similar to the quartz particles of modern eolian deposits in the western Qaidam Basin.

In contrast, the second type of Facies IV sediments (lower part of Figure 2d) contains faint silt layers. The grain size distributions of the second type of Facies IV sediments show a bimodal distribution with coarse and fine components, indicative for a mixture of depositional processes including strong fluvial and eolian input. This interpretation is supported by the SEM examination on quartz-grain morphology and surface texture and by comparison with modern eolian quartz particles from the same region (Figure 3b; core depth: 76.85 m).

Facies V is characterized by mudstones containing evaporitic fragments along with relatively low organic matter (6–13% of LOI-550 °C) but high carbonate (12–25% of LOI-950 °C; Figure 2e) contents. The evaporitic fragments are commonly floating in the mud and show a scattered distribution (Figures 2e and $2e_1$), implying that the evaporites are not formed in situ. While no indication for a far onshore energetic mass transport

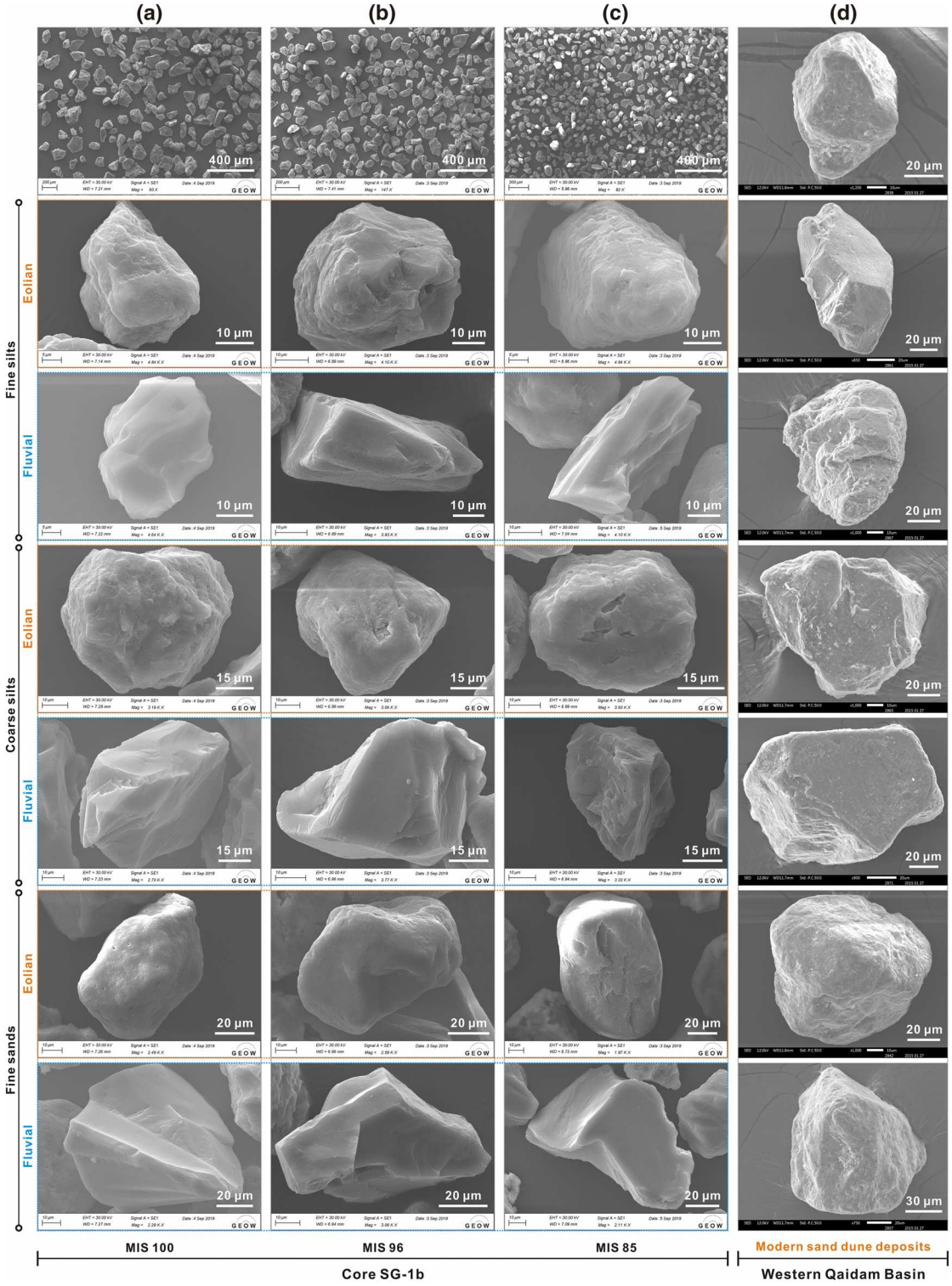

Figure 3. Comparison of representative quartz particles from Facies IV of Core SG-1b (a–c) with modern eolian grains from the western Qaidam Basin (d). Representative quartz grains from (a) glacial MIS 100 (core depth: 80.85 m), (b) glacial MIS 96 (core depth: 76.85 m), (c) interglacial MIS 85 (core depth: 65.53 m), and (d) quartz grains from modern sand dune deposits in Youshashan, western Qaidam Basin (see Figure 1b for location).

source of these evaporite fragments (e.g., slumping or the occurrence of an erosional base) can be observed, we rather interpret these fragments to result from local storm deposits. The evaporitic fragments were most probably sourced from the top area of the Jianshan anticline, where evaporites could form in shallower

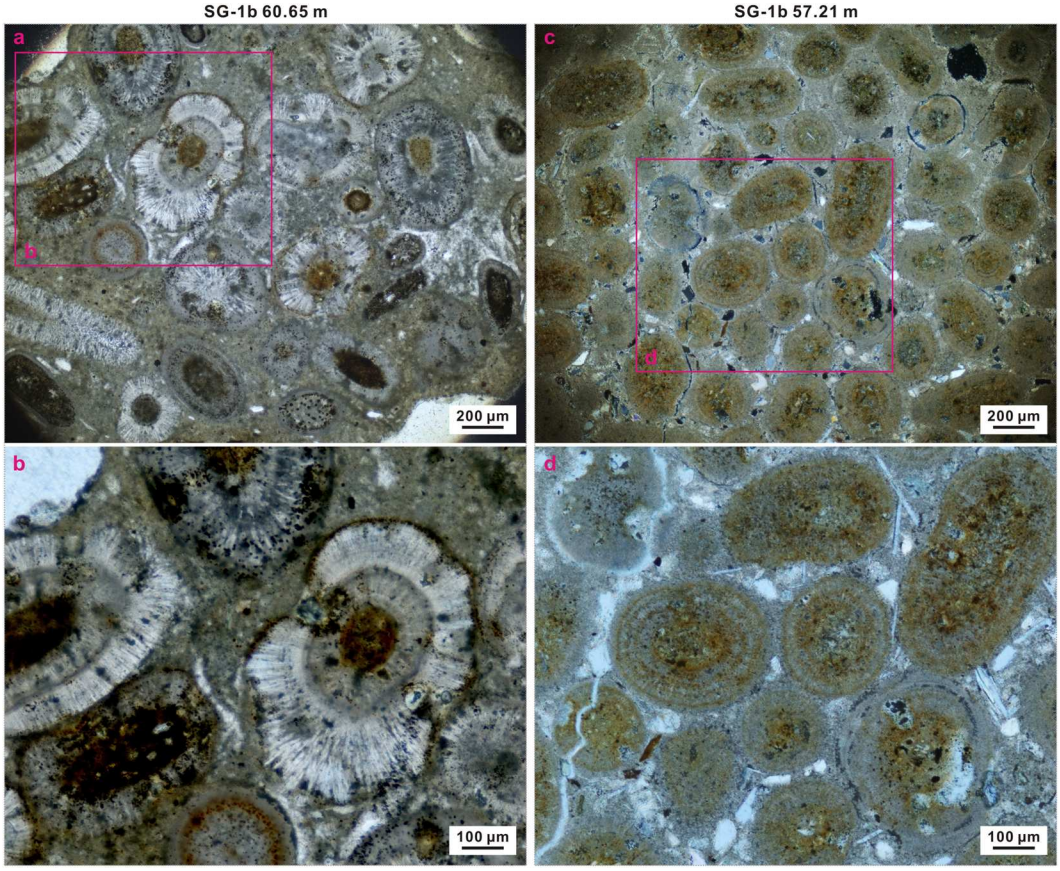

Figure 4. Photomicrograph of representative thin sections showing ooids in Core SG-1b. Sample depth: (a) and (b) 60.65 m (~2251 ka); (c) and (d) 57.21 m (~2175 ka).

water depths. During storm events, these evaporites could have been eroded and transported into the deeper part of the Qaidam lake by storm waves.

Facies VI shows the presence of ooids within the mudstones (Figure 2f). These ooids are small (mm in diameter, Figure $2f_1$), coated sedimentary grains of spheroidal shape that are composed out of calcium carbonate (Figure 4). This is also reflected by the high carbonate content (10–31% of LOI-950 °C) of this facies accompanied by relatively low organic matter content (5–13% of LOI-550 °C) (Figure 2e). Ooids are generally formed on a wave-washed bench and deposited on the lakeward dipping slope during periods of high wave activity (Talbot & Allen, 1996). Since there is a lack of sedimentary structures that would infer a mass transport source of these ooids, we interpret these ooids to be formed in situ. This interpretation would indicate a very shallow lake environment with wind-induced wave activity at the drill site.

Facies VII comprises of evaporitic sediments that are preserved as gray-colored hard rocks. These sediments are characterized by the highest carbonate content (16–35% of LOI-950 °C) and the lowest organic matter content (3–11% of LOI-550 °C) of the described lithofacies types (Figure 2g). Previous investigations on lacustrine sediments (~2.8–0 Ma) in the neighboring Core SG-1 (Figure 1b), located about 30 km NE from Core SG-1b, reveal that comparable evaporites were deposited under dry climate conditions and during periods of decreasing lake levels (Li et al., 2010; Wang et al., 2012). We therefore interpret the presence of Facies VII to represent dry climate conditions resulting in enhanced evaporation and a drop of the Qaidam paleolake level.

4.2. End-Member Modeling of Grain Size Distributions

Using the coefficient of determination, our EMMA results show three end members to be the optimal number required to subdivide the grain size curves of Core SG-1b sediments into significant sediment

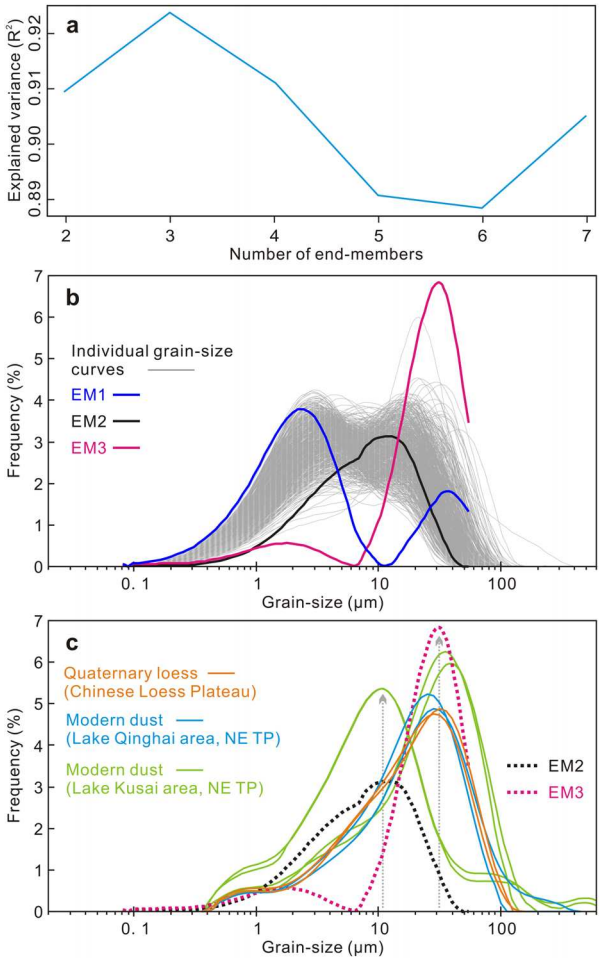

Figure 5. End-member (EM) modeling results for the sediments between 100.45 m and 56.45 m of Core SG-1b. (a) Explained variance (R^2) of all size classes for each end-member model; modeling with three EMs is the best fit for the SG-1b grain-size data set. (b) Modeled EM (bold curves) from the measured grain size data set; grain size distribution curves of all samples from Core SG-1b are plotted as gray curves. (c) Comparison of EMs 2 and 3 (dotted lines) with grain size distribution curves of modern dust from the Lake Qinghai catchment area (light blue) to the east of the Qaidam Basin, NE Tibetan Plateau (TP) (An et al., 2012), modern dust from Lake Kusai catchment (light green), NE TP (Liu et al., 2009), and Quaternary loess from Luochuan section (orange), Chinese Loess Plateau (Vandenberghe et al., 1997).

subpopulations, that is, end-members (EM) (Figure 5a). EM 1 has a major mode at ~2 μm and a minor mode at ~40 μm. EM 2 shows a unimodal distribution with the mode at ~12 μm, and EM 3 shows a major and a minor mode at ~32 and ~ 2 μm, respectively (Figure 5b). When plotted against the available age model, EM1 shows similar fluctuations to the downcore distribution of grain sizes <4 μm, while EM2 and EM3 are comparable to the distribution of the grain sizes 4–32 μm and >32 μm, respectively (Figure S2 in the supporting information).

The modeled EMs from SG-1b show large similarities to grain size distribution curves from the region (Figure 5c). Specifically, EM 3 is similar to grain size distribution curves of modern dust from the Lake Qinghai catchment to the east of the Qaidam Basin (An et al., 2012), modern dust from the Lake Kusai catchment (Liu et al., 2009), and Quaternary loess from the Luochuan section, Chinese Loess Plateau (Vandenberghe et al., 1997), suggesting an eolian source of this EM. The modeled EM2 is also comparable to modern dust from the Lake Kusai catchment (Liu et al., 2009). The EM 1 is comparable to suspended particles in a modern river that drains to Lake Qinghai (An et al., 2012), implying fluvial input of suspension particles to the drilling site.

4.3. Glacial-Interglacial Climate Fluctuations

The LOI-550 °C and LOI-950 °C have been used in several studies to estimate the organic matter and carbonate content of lacustrine sequences on the NE Tibetan Plateau (Herzschuh et al., 2009; Mischke et al., 2005). The organic matter content of lake sediments is mainly controlled by biomass production within the lake and the lake catchment area, and the decomposition of organic material within the water body. Previous studies have shown that the NE Tibetan Plateau was characterized by dry and cold climate conditions during glacial intervals of the Pleistocene (Herb et al., 2015; Koutsodendris et al., 2018; Zhang et al., 2019). These climatic conditions were driven by a strong EAWM causing the decrease of biomass production within the lake and the lake catchment area (Aichner et al., 2012; Herzschuh et al., 2009; Mischke et al., 2005). Based on these arguments, LOI-550 °C minima in the SG-1b record can be interpreted to represent glacial intervals, while LOI-550 °C maxima represent interglacial conditions.

The main carbonate source of the Qaidam paleolake is supposed to be authigenic (Herb et al., 2013; Li et al., 2010). Detailed examinations of the long-term lithological variation and mineral formation over the past 2.8 Ma in the western Qaidam Basin show that an increase in the carbonate content of the sediments is resulting from enhanced evaporation and lowering of the lake level under dry climate conditions (Li et al., 2010; Wang et al., 2012). In the present study, we therefore interpret LOI-950 °C maxima to be representative for an arid climate and low lake levels. The negative correlation between LOI-550 °C and LOI-950 °C (Figures 6d and 6e) further supports the interpretation that the LOI-950 °C and LOI-550 °C maxima indicate dry and humid climate conditions, respectively.

In the Qaidam paleolake, strong winds (Kapp et al., 2011; Pullen et al., 2011; Qiang et al., 2007) and fluvial input (Lu et al., 2015; Wang et al., 2012) are the main contributors of clastic particle transport into the lake. During dry and cold glacial periods that are dominated by a strong EAWM (Herb et al., 2015; Koutsodendris et al., 2018), a lowering of the lake level will lead to the exposure of previously submerged areas that are covered with loose nearshore sediments. Because these sediments are generally coarser than those in the central zone of the lake (Lu et al., 2018) and exposed to wind- and wave-driven erosion, this would lead to increasing proximal eolian and fluvial input of coarser grains into the Qaidam paleolake. In addition, the cold and dry

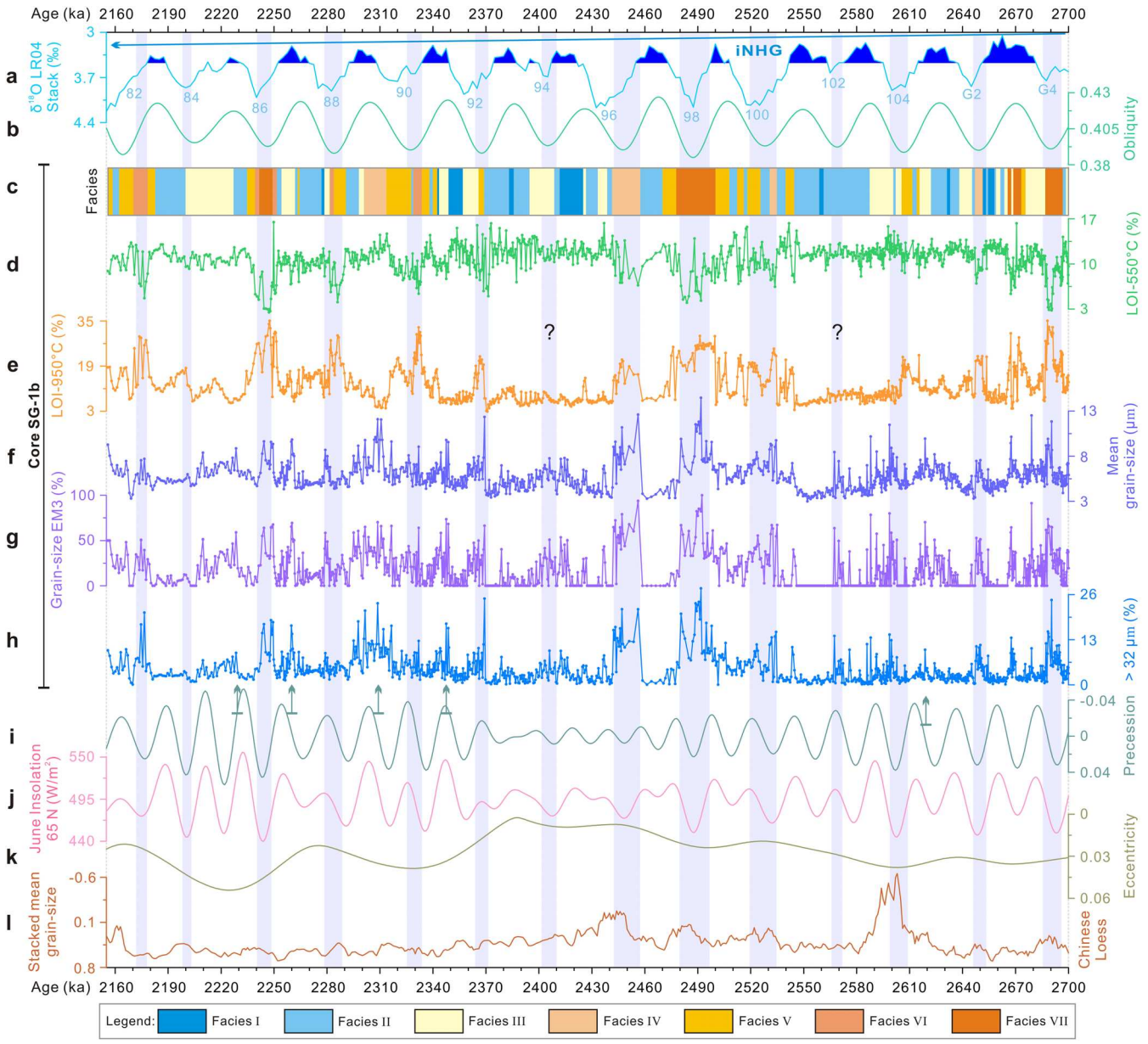

Figure 6. Comparison of proxy records from Core SG-1b, western Qaidam Basin (c–g) plotted against the global benthic foraminiferal $\delta^{18}O$ stack (a), orbital parameters (b, i, j, and k) and grain size from the Chinese Loess Plateau (l). (a) The LR04 stack for the interval between MIS G4 and 82 (Lisiecki & Raymo, 2005); iNHG = intensification of Northern Hemisphere glaciation. (b) Orbital obliquity from the La2004 solution (Laskar et al., 2004). (c) Facies distribution of Core SG-1b. (d) Loss on ignition (LOI) of sediments at 550 °C (indicating organic matter content) in Core SG-1b. (e) LOI-950 °C (indicating carbonate content) in Core SG-1b. (f) Mean grain size of sediments in Core SG-1b. (g) Content of grain size EM3 in Core SG-1b. (h) Content of coarse silt and fine sand in Core SG-1b. (i), (j), and (k) orbital precession (light green) from the La2004 solution, summer insolation (pink), and eccentricity (gray) (Laskar et al., 2004); the light green arrows indicate grain size coarsening within interglacials, corresponding to strengthened East Asian summer monsoon (EASM) precipitation. (l) Stacked loess mean grain size from the Chinese Loess Plateau (Sun et al., 2006). The "?" indicates weakly expressed glacials in the Core SG-1b record.

glacial climate conditions would enhance dust input from distal sources via dust storms. This process gains support from observations of dust in ice cores from the NE Tibetan Plateau during the Little Ice Age (~1400 AD to ~1700 AD) (Thompson et al., 1995; Yang et al., 2007). We assume even stronger dust storms under the cold and dry conditions of glacial times. The distinct yellowish-gray millimeter-thick silty layers of Facies III might result from such a depositional process, reflecting increased dust storm activity

(Figure 2c). Therefore, we interpret an increase in Core SG-1b grain sizes (Figure 6) to reflect a combination of both proximal transport of former lake shore sediments and increased eolian input. The observed mixed occurrence of quartz grains showing both eolian and fluvial microtextures (see Figure 3) within the intervals of larger grain sizes supports this interpretation.

In addition to the abovementioned processes, rare floods with higher discharge (strong fluvial input) in the basin during dry climate periods with shallower lake level might be an additional mechanism to deliver coarser particles to the central zone of the lake during glacials, thereby contributing to a coarsening of grain sizes in Core SG-1b sediments. The relative portion of very large water discharges is much higher in arid regions than in more humid regions as documented by the analysis of annual peak water discharges and average daily water discharges of 440 American streams spanning a wide range of climates (Molnar, 2001; Molnar et al., 2006). Meteorological data from the Dead Sea drainage basin, Southern Levant also shows that the frequency of floods in arid regions is much higher than in humid regions and the relative portion of higher rainfall intensities increases with the reduction of annual rainfall amounts (Ben-Zvi, 1988; Greenbaum et al., 1998). A recently published flood record from the Dead Sea spanning the last 45 kyr also shows small-magnitude but high-frequency floods during the humid Last Glacial, while the less humid Holocene is characterized by low-frequency but large-magnitude floods (Lu et al., 2020).

Irrespective of the processes involved (i.e., dust storms, flood events, and/or proximal input by wind- and wave-driven currents), an increase in grain size within the Core SG-1b record can be generally interpreted to represent dry climate conditions, an interpretation that is supported by the observed minima in LOI-550 °C and maxima in LOI-950 °C. In contrast, interglacials are generally characterized by smaller grain sizes (typically with mean sizes around 3 to 5 μm; Figure 6f). This grain size clearly separates in the end-member modeling (EM1) and can be interpreted as typical for increased fluvial input under a warm and wet climate on the Tibetan Plateau, an interpretation supported by studies from this area (An et al., 2012; Dietze et al., 2012; Dietze et al., 2014).

Overall, the LOI and grain size derived paleoclimate record from Core SG-1b demonstrates a pronounced glacial-interglacial cyclicity between 2.7 and 2.1 Ma that generally follows the global benthic foraminiferal $\delta^{18}O$ stack (Figure 6). Interglacial (glacial) periods are thereby characterized by smaller (coarser) grain size, maxima (minima) in LOI-550 °C, and minima (maxima) in LOI-950 °C. Exceptions from this general pattern are the time periods 2630–2615 ka, 2350–2340 ka, 2315–2295 ka, 2265–2255 ka, and 2230–2210 ka, which are located within the interglacials MIS G1, 91, 89, 87, and 85, respectively (indicated by the arrows in Figures 6f–6h). During these interglacials, sediments are composed out of Facies I to IV and show relatively high organic matter (8–15% of LOI-550 °C) and low carbonate contents (4–15% of LOI-950 °C; Figure 2e). While this is similar to other interglacials; however, these specific intervals are characterized by relatively coarse grain sizes, with a mean grain size of 5–12 μm (Figure 6f).

These out-of-the-order grain size coarsening events within interglacials correspond well with insolation maxima paced by orbital eccentricity (arrows in Figures 6h and 6j), an observation that is supported by recent studies that infer an increased imprint of eccentricity, and in association precession, in the Qaidam Basin under high eccentricity amplitudes (Luo et al., 2018; Su et al., 2019; Su et al., 2019). During eccentricity maxima the amplitude of precession is larger, causing a summer season lengthening and thus potentially enhanced EASM precipitation (Berger, 1988; Braconnot et al., 2008). In contrast to the general sedimentation of smaller particles during interglacials, this process is proposed to trigger an increase of fluvial input and hence the deposition of coarser-grained sediments on the NE Tibetan Plateau, an interpretation supported by the SEM observation within one of these intervals (2230–2210 ka, MIS 85; Figure 3c). In fact, previous findings based on eolian deposits on the Chinese Loess Plateau also revealed enhanced EASM precipitation during the time periods 2.75–2.58 Ma and 2.35–2.20 Ma (Sun et al., 2010), which coincide with the interglacial grain size coarsening intervals recorded in our paleoenvironmental records. In addition, grain size and total organic carbon records from the Kusai Lake (Figure 1b) (Liu et al., 2009) and the central Qaidam Basin (Nie et al., 2017) reveal that EASM precipitation penetrated further inland to the nearby region of our study area during the Late Holocene and Late Miocene, respectively. A similar penetration of the EASM into the inland of Central Asia during the mid-Holocene has been reported in $\delta^{18}O$ records of stalagmites from Kesang Cave (Figure 1a), Tianshan Mountains (Cheng et al., 2012). Therefore, we infer that at least partly a northward penetration of the EASM increased precipitation during these interglacials.

In addition, westerlies might also serve as a potential moisture source to the interglacial Qaidam Basin (Caves et al., 2015; Yao et al., 2013) as discussed in detail below (section 4.4).

4.4. Primary Forcing Mechanisms of Glacial–Interglacial Climatic Fluctuations

Thick and continuous Chinese loess sequences in northern China provide an important archive for paleoclimate reconstructions. Grain size records of these loess sequences demonstrate a clear link between high-latitude Northern Hemisphere climate and climate fluctuations in midlatitude northern China on glacial-interglacial time scales (Ding et al., 1995; Ding et al., 2002; Hao et al., 2012; Sun et al., 2011; Sun & An, 2004; Vandenberghe et al., 1997). Especially the pronounced glacials MIS G4, 100, 98, 96, 92, and 86, that are recorded in Core SG-1b by increasing grain size (Figures 6f–6h), can be correlated to intervals of coarsening in the stacked mean grain size of the Chinese loess record (Figure 6l) (Sun et al., 2006). Since this stacked grain size record is a first-order indicator of EAWM variation (coarse grain size representing strong EAWM and vice versa) (Ding et al., 2002; Sun et al., 2006; Sun et al., 2010), the correlation between the SG-1b record and the Chinese loess record suggests a key role of the EAWM and thus a high-latitude Northern Hemisphere climate component on NE Tibetan paleoclimate.

Previous records of late Holocene lacustrine sequences from Kusai Lake (Figure 1b) reveal a strong influence of the EAWM on NE Tibetan Plateau climate at centennial time scales (Liu et al., 2009). Periods of strong EAWM are thereby characterized by low total organic carbon content in Lake Kusai sediments because cold temperatures and low precipitation lead to low primary productivity in the lake (Liu et al., 2009). Furthermore, eolian sequences that have been deposited during the last 30 kyr in the Xining Basin (Figure 1a), NE Tibetan Plateau (Wang et al., 2015) and Holocene sedimentary records from the Genggahai Lake, eastern Qaidam Basin (Qiang et al., 2014), suggest a major influence of the EAWM on the regional climate on millennial time scales as evidenced by dust accumulation and intense sand deposition events that can be correlated to cooling events in the high northern latitudes. Being strong even during cool and dry episodes of the Holocene (see above) implies that the EAWM is expected to be even stronger on glacial-interglacial time scales. Geochemical records of Core SG-1 (Figure 1b) for the last 600 kyr demonstrate an EAWM forcing on regional climate (Yang et al., 2017) with a low lake level and increased deposition of evaporites during glacials due to low precipitation under arid climate conditions (Herb et al., 2015; Koutsodendris et al., 2018).

Variations in the Northern Hemisphere ice sheet volume directly influence the Siberian High and therefore variations in the EAWM (Ding et al., 1995; Hao et al., 2012). During glacials, the general increase in ice volume intensified the Siberian High and, consequently, strengthened the EAWM. In addition, the cooling of upper-ocean temperatures in the surrounding oceans may have led to reduced moisture supply to the continental interiors (Dupont-Nivet et al., 2007). Both processes would have led to enhanced aridification in the western Qaidam Basin during glacial periods (Figure 7). In Core SG-1b these dry glacials are expressed by intervals with low organic matter content, high carbonate content and coarse grain size (Figure 6).

During interglacials, the reduced Northern Hemisphere ice volume would have weakened the Siberian High and the EAWM. Consequently, the western Qaidam Basin would have been less influenced by the EAWM, leading to wetter conditions compared to glacials (Herb et al., 2015) as shown by intervals with high organic matter content, low carbonate content, and finer grain size in the SG-1b record (Figure 6).

With the weakening influence of the EAWM on the Qaidam Basin during interglacials, the influence of the westerlies might also have strengthened substantially. The westerlies play an important role in delivering moisture from the Atlantic Ocean and the Mediterranean into Central Asia (Caves et al., 2015; Yao et al., 2013). Meteorological data reveal that the current westerlies have different routes across Central Asia during the warm summer-half year than compared to the cold winter-half year (Schiemann et al., 2009). In summer, the mainstream of the westerlies crosses the region through the northern edge of the Tibetan Plateau. During winter, in contrast, the westerlies are shifted equatorward and split into two branches when encountering the high Tibetan Plateau (An et al., 2011; Chiang et al., 2015); one along the southern edge of the plateau and the other one along the northern edge of the plateau (Figure 1a). Global climate modeling (Shin et al., 2003; Toggweiler & Russell, 2008; Williams & Bryan, 2006) and atmospheric observations (Han et al., 2008; Nagashima et al., 2011; Zhang & Liu, 2018) support this seasonal shift in the mainstream of the westerlies.

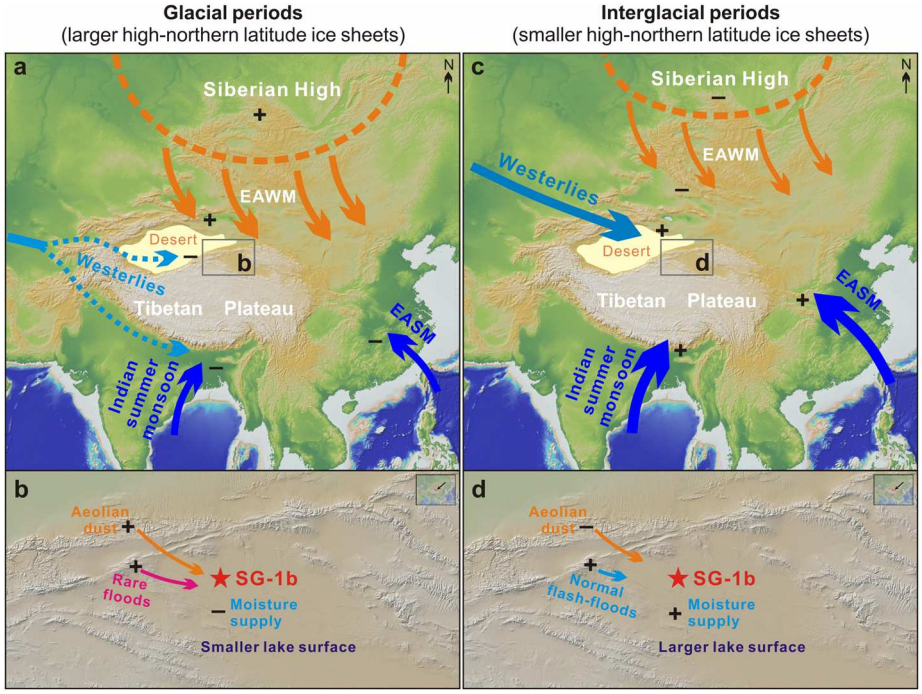

Figure 7. Schematic model illustration of the proposed forcing of the (a, b) glacial-(c, d) interglacial climate fluctuations recorded in Core SG-1b sediments during the latest Pliocene to early Pleistocene. The "+" and "−" refer to the enhancement and reduction of a target process, respectively.

The modern seasonal scenario of the westerlies appears to be a reasonable analog for the behavior of the westerlies during Quaternary glacial–interglacial cycles (Kapp et al., 2011; Pullen et al., 2011). During glacial periods, the expansion of northern latitude ice sheets strengthens the polar jet streams (EAWM) (Kapp et al., 2011; Pullen et al., 2011) and shifts the westerlies southward, leading to a decreased influence over the NE Tibetan Plateau (Figures 7a and 7b). This equatorward migration of both the polar jet and the westerlies might have suppressed the delivery of moisture to the NE Tibetan Plateau and thus enhanced the observed aridification in the study area. This is exemplified by the low organic matter content and the coarser grain sizes during glacials in Core SG-1b (Figure 6f). During interglacial periods, in contrast, the NE Tibetan Plateau would have been characterized by a larger influence of both the westerlies and the EASM, delivering more moisture to the region (Figures 7c and 7d). This is reflected by the high organic matter content and the finer grain sizes during interglacials in Core SG-1b (Figure 6f). Based on these lines of arguments, we conclude that the glacial-interglacial climate fluctuations recorded in the Core SG-1b sediments are primarily forced by the waning and waxing of Northern Hemisphere ice sheets across the iNHG.

5. Conclusions

High-resolution (~500 years) LOI and grain size records from Core SG-1b show pronounced glacial–interglacial climate fluctuations that have occurred on the NE Tibetan Plateau during the latest Pliocene and early Pleistocene (2.7–2.1 Ma). Our study infers a link between the observed glacial-interglacial climate fluctuations with the waning and waxing of ice sheets across the intensification of Northern Hemisphere glaciation. The close accordance between the SG-1b record with the LR04 stack, Earth's orbital parameters, and the Chinese loess record suggests that iNHG is the primary driver of the observed glacial-interglacial climatic fluctuations through its influence on the Siberian High pressure system and, in turn, the East Asian winter monsoon. The observed climatic fluctuations are thereby enabled by the high topography of the Tibetan Plateau via modifying the position and intensity of westerlies over the region on glacial–interglacial time scales.

Acknowledgments

Funding for this study has been provided by the German Research Foundation (DFG; Grants FR2544/13-1 to O. F. and KO4960/4 to A. K.). We thank F. Allstädt, A. Bahr, H. Campos, T. Fischer, O. Kern, K. S. Nakajima, and H. Schulz for their technical and logistic support. We declare no conflict of interests. Three anonymous reviewers are thanked for providing helpful and constructive comments, which improved the quality of the manuscript substantially. All analytical data presented here are available electronically in the supporting information and PANGAEA database at PANGAEA (https://doi.pangaea.de/10.1594/PANGAEA.904079).

References

Aichner, B., Herzschuh, U., Wilkes, H., Schulz, H.-M., Wang, Y., Plessen, B., et al. (2012). Ecological development of Lake Donggi Cona, north-eastern Tibetan plateau, since the late glacial on basis of organic geochemical proxies and non-pollen palynomorphs. *Palaeogeography, Palaeoclimatology, Palaeoecology*, *313-314*, 140–149. https://doi.org/10.1016/j.palaeo.2011.10.015

An, Z., Clemens, S. C., Shen, J., Qiang, X., Jin, Z., Sun, Y., et al. (2011). Glacial-interglacial Indian summer monsoon dynamics. *Science*, *333*(6043), 719–723. https://doi.org/10.1126/science.1203752

An, Z., Colman, S. M., Zhou, W., Li, X., Brown, E. T., Jull, A. J. T., et al. (2012). Interplay between the westerlies and Asian monsoon recorded in Lake Qinghai sediments since 32 ka. *Scientific Reports*, *2*(1), 1, 619–7. https://doi.org/10.1038/srep00619

An, Z., Kutzbach, J. E., Prell, W. L., & Porter, S. C. (2001). Evolution of Asian monsoons and phased uplift of the Himalaya-Tibetan plateau since Late Miocene times. *Nature*, *411*(6833), 62–66.

Bartoli, G., Sarnthein, M., & Weinelt, M. (2006). Late Pliocene millennial-scale climate variability in the northern North Atlantic prior to and after the onset of Northern Hemisphere glaciation. *Paleoceanography*, *21*(4). https://doi.org/10.1029/2005pa001185

Ben-Zvi, A. (1988). Maximal discharges observed in Israel. *Environmental Geology and Water Sciences*, *11*(1), 15–19.

Berger, A. (1988). Milankovitch theory and climate. *Reviews of Geophysics*, *26*(4), 624–657.

Blott, S. J., & Pye, K. (2001). GRADISTAT: A grain size distribution and statistics package for the analysis of unconsolidated sediments. *Earth Surface Processes and Landforms*, *26*(11), 1237–1248.

Braconnot, P., Marzin, C., Grégoire, L., Mosquet, E., & Marti, O. (2008). Monsoon response to changes in Earth's orbital parameters: Comparisons between simulations of the Eemian and of the Holocene. *Climate of the Past*, *4*, 281–294.

Cai, M., Fang, X., Wu, F., Miao, Y., & Appel, E. (2012). Pliocene-Pleistocene stepwise drying of Central Asia: Evidence from paleomagnetism and sporopollen record of the deep borehole SG-3 in the western Qaidam Basin, NE Tibetan Plateau. *Global and Planetary Change*, *94-95*, 72–81. https://doi.org/10.1016/j.gloplacha.2012.07.002

Caves, J. K., Winnick, M. J., Graham, S. A., Sjostrom, D. J., Mulch, A., & Chamberlain, C. P. (2015). Role of the westerlies in Central Asia climate over the Cenozoic. *Earth and Planetary Science Letters*, *428*, 33–43. https://doi.org/10.1016/j.epsl.2015.07.023

Chen, J., An, Z., & Head, J. (1999). Variation of Rb/Sr ratios in the loess-paleosol sequences of central China during the last 130,000 years and their implications for monsoon paleoclimatology. *Quaternary Research*, *51*(3), 215–219.

Cheng, H., Zhang, P. Z., Spötl, C., Edwards, R. L., Cai, Y. J., Zhang, D. Z., et al. (2012). The climatic cyclicity in semiarid-arid central Asia over the past 500,000 years. *Geophysical Research Letters*, *39*, L01705. https://doi.org/10.1029/2011gl050202

Chiang, J. C. H., Fung, I. Y., Wu, C.-H., Cai, Y., Edman, J. P., Liu, Y., et al. (2015). Role of seasonal transitions and westerly jets in east Asian paleoclimate. *Quaternary Science Reviews*, *108*, 111–129. https://doi.org/10.1016/j.quascirev.2014.11.009

De Schepper, S., Gibbard, P. L., Salzmann, U., & Ehlers, J. (2014). A global synthesis of the marine and terrestrial evidence for glaciation during the Pliocene epoch. *Earth-Science Reviews*, *135*, 83–102. https://doi.org/10.1016/j.earscirev.2014.04.003

Dean, W. E. (1974). Determination of carbonate and organic matter in calcareous sediments and sedimentary rocks by loss on ignition; comparison with other methods. *Journal of Sedimentary Research*, *44*(1), 242–248.

Demenocal, P. B. (2004). African climate change and faunal evolution during the Pliocene-Pleistocene. *Earth and Planetary Science Letters*, *220*(1), 3–24.

Dietze, E., Hartmann, K., Diekmann, B., Ijmker, J., Lehmkuhl, F., Opitz, S., et al. (2012). An end-member algorithm for deciphering modern detrital processes from lake sediments of Lake Donggi Cona, NE Tibetan Plateau, China. *Sedimentary Geology*, *243-244*, 169–180. https://doi.org/10.1016/j.sedgeo.2011.09.014

Dietze, E., Maussion, F., Ahlborn, M., Diekmann, B., Hartmann, K., Henkel, K., et al. (2014). Sediment transport processes across the Tibetan Plateau inferred from robust grain-size end members in lake sediments. *Climate of the Past*, *10*(1), 91–106. https://doi.org/10.5194/cp-10-91-2014

Ding, Z., Liu, T., Rutter, N. W., Yu, Z., Guo, Z., & Zhu, R. (1995). Ice-volume forcing of East Asian winter monsoon variations in the past 800,000 years. *Quaternary Research*, *44*(2), 149–159.

Ding, Z. L., Derbyshire, E., Yang, S. L., Yu, Z. W., Xiong, S. F., & Liu, T. S. (2002). Stacked 2.6-Ma grain size record from the Chinese loess based on five sections and correlation with the deep-sea $\delta^{18}O$ record. *Paleoceanography*, *17*(3), 1033. https://doi.org/10.1029/2001pa000725

Dupont-Nivet, G., Krijgsman, W., Langereis, C. G., Abels, H. A., Dai, S., & Fang, X. (2007). Tibetan plateau aridification linked to global cooling at the Eocene–Oligocene transition. *Nature*, *445*(7128), 635–638. https://doi.org/10.1038/nature05516

Fang, X., Zhang, W., Meng, Q., Gao, J., Wang, X., King, J., et al. (2007). High-resolution magnetostratigraphy of the Neogene Huaitoutala section in the eastern Qaidam Basin on the NE Tibetan Plateau, Qinghai Province, China and its implication on tectonic uplift of the NE Tibetan Plateau. *Earth and Planetary Science Letters*, *258*(1-2), 293–306. https://doi.org/10.1016/j.epsl.2007.03.042

Friedrich, O., Wilson, P. A., Bolton, C. T., Beer, C. J., & Schiebel, R. (2013). Late Pliocene to early Pleistocene changes in the North Atlantic Current and suborbital-scale sea-surface temperature variability. *Paleoceanography*, *28*(2), 274–282. https://doi.org/10.1002/palo.20029

Gao, Y., Xu, S., Guo, Q., & Zhang, M. (1962). Monsoon region and regional climate in China. In X. Gao, & S. Xu (Eds.), *Some questions of East Asian monsoon (in Chinese)*, (pp. 49–63). Beijing: Science Press.

Grant, K. M., Rohling, E. J., Westerhold, T., Zabel, M., Heslop, D., Konijnendijk, T., & Lourens, L. (2017). A 3 million year index for North African humidity/aridity and the implication of potential pan-African humid periods. *Quaternary Science Reviews*, *171*, 100–118. https://doi.org/10.1016/j.quascirev.2017.07.005

Greenbaum, N., Margalit, A., Schick, A. P., Sharon, D., & Baker, V. R. (1998). A high magnitude storm and flood in a hyperarid catchment, Nahal Zin, Negev Desert, Israel. *Hydrological Processes*, *12*(1), 1–23.

Han, Y., Fang, X., Kang, S., Wang, H., & Kang, F. (2008). Shifts of dust source regions over central Asia and the Tibetan Plateau: Connections with the Arctic oscillation and the westerly jet. *Atmospheric Environment*, *42*(10), 2358–2368. https://doi.org/10.1016/j.atmosenv.2007.12.025

Hao, Q., Wang, L., Oldfield, F., Peng, S., Qin, L., Song, Y., et al. (2012). Delayed build-up of Arctic ice sheets during 400,000-year minima in insolation variability. *Nature*, *490*(7420), 393–396. https://doi.org/10.1038/nature11493

Heiri, O., Lotter, A. F., & Lemcke, G. (2001). Loss on ignition as a method for estimating organic and carbonate content in sediments: Reproducibility and comparability of results. *Journal of Paleolimnology*, *25*(1), 101–110.

Herb, C., Koutsodendris, A., Zhang, W., Appel, E., Fang, X., Voigt, S., & Pross, J. (2015). Late Plio-Pleistocene humidity fluctuations in the western Qaidam Basin (NE Tibetan Plateau) revealed by an integrated magnetic-palynological record from lacustrine sediments. *Quaternary Research*, *84*(3), 457–466. https://doi.org/10.1016/j.yqres.2015.09.009

Herb, C., Zhang, W., Koutsodendris, A., Appel, E., Fang, X., & Pross, J. (2013). Environmental implications of the magnetic record in Pleistocene lacustrine sediments of the Qaidam Basin, NE Tibetan Plateau. *Quaternary International*, *313-314*, 218–229. https://doi.org/10.1016/j.quaint.2013.06.015

Herzschuh, U., Mischke, S., Meyer, H., Plessen, B., & Zhang, C. (2009). Using variations in the stable carbon isotope composition of macrophyte remains to quantify nutrient dynamics in lakes. *Journal of Paleolimnology*, *43*(4), 739–750. https://doi.org/10.1007/s10933-009-9365-0

Hill, D. J., Bolton, K. P., & Haywood, A. M. (2017). Modelled ocean changes at the Plio-Pleistocene transition driven by Antarctic ice advance. *Nature Communications*, *8*(1), 1–8. https://doi.org/10.1038/ncomms14376

Jakob, K. A., Bolton, C. T., Wilson, P. A., Bahr, A., Pross, J., Fiebig, J., & Friedrich, O. (2017). Glacial-interglacial changes in equatorial Pacific surface-water structure during the Plio-Pleistocene intensification of Northern Hemisphere Glaciation. *Earth and Planetary Science Letters*, *463*, 69–80. https://doi.org/10.1016/j.epsl.2017.01.028

Kaboth-Bahr, S., Koutsodendris, A., Lu, Y., Nakajima, K., Zeeden, C., Appel, E., et al. (2020). A late Pliocene to early Pleistocene (3.3–2.1 Ma) orbital chronology for the Qaidam Basin paleolake (NE Tibetan Plateau) based on the SG-1b drillcore record. *Newsletters on Stratigraphy*. https://doi.org/10.1127/nos/2020/0555

Kapp, P., Pelletier, J. D., Rohrmann, A., Heermance, R., Russell, J., & Ding, L. (2011). Wind erosion in the Qaidam basin, Central Asia: Implications for tectonics, paleoclimate, and the source of the Loess Plateau. *GSA Today*, *21*(4), 4–10. https://doi.org/10.1130/gsatg99a.1

Kleiven, H. F., Jansen, E., Fronval, T., & Smith, T. (2002). Intensification of Northern Hemisphere glaciations in the circum Atlantic region (3.5–2.4 Ma)—Ice-rafted detritus evidence. *Palaeogeography, Palaeoclimatology, Palaeoecology*, *184*(3–4), 213–223.

Konert, M., & Vandenberghe, J. (1997). Comparison of laser grain size analysis with pipette and sieve analysis: A solution for the under-estimation of the clay fraction. *Sedimentology*, *44*(3), 523–535.

Koutsodendris, A., Allstädt, F. J., Kern, O. A., Kousis, I., Schwarz, F., Vannacci, M., et al. (2019). Late Pliocene vegetation turnover on the NE Tibetan plateau (Central Asia) triggered by early Northern Hemisphere glaciation. *Global and Planetary Change*, *180*, 117–125. https://doi.org/10.1016/j.gloplacha.2019.06.001

Koutsodendris, A., Sachse, D., Appel, E., Herb, C., Fischer, T., Fang, X., & Pross, J. (2018). Prolonged monsoonal moisture availability preconditioned glaciation of the Tibetan Plateau uring the mid-Pleistocene transition. *Geophysical Research Letters*, *45*, 13,020–13,030. https://doi.org/10.1029/2018gl079303

Laskar, J., Robutel, P., Joutel, F., Gastineau, M., Correia, A., & Levrard, B. (2004). A long-term numerical solution for the insolation quantities of the Earth. *Astronomy & Astrophysics*, *428*(1), 261–285.

Li, J., Fang, X., Song, C., Pan, B., Ma, Y., & Yan, M. (2014). Late Miocene-quaternary rapid stepwise uplift of the NE Tibetan Plateau and its effects on climatic and environmental changes. *Quaternary Research*, *81*(3), 400–423.

Li, M., Fang, X., Yi, C., Gao, S., Zhang, W., & Galy, A. (2010). Evaporite minerals and geochemistry of the upper 400 m sediments in a core from the Western Qaidam Basin, Tibet. *Quaternary International*, *218*, 176–189. https://doi.org/10.1016/j.quaint.2009.12.013

Li, Z., Yan, G., Yamin, W., Yanhui, P., Jianguo, L., Aifang, C., et al. (2015). Can monsoon moisture arrive in the Qilian Mountains in summer? *Quaternary International*, *358*, 113–125. https://doi.org/10.1016/j.quaint.2014.08.046

Lisiecki, L. E., & Raymo, M. E. (2005). A Pliocene-Pleistocene stack of 57 globally distributed benthic $\delta^{18}O$ Records. *Paleoceanography*, *20*, PA1003. https://doi.org/10.1029/2004pa001071

Liu, X., Dong, H., Yang, X., Herzschuh, U., Zhang, E., Stuut, J.-B. W., & Wang, Y. (2009). Late Holocene forcing of the Asian winter and summer monsoon as evidenced by proxy records from the northern Qinghai-Tibetan Plateau. *Earth and Planetary Science Letters*, *280*, 276–284. https://doi.org/10.1016/j.epsl.2009.01.041

Lu, H., Wang, X., Ma, H., Tan, H., Vandenberghe, J., Miao, X., et al. (2004). The plateau monsoon variation during the past 130 kyr revealed by loess deposit at northeast Qinghai-Tibet (China). *Global and Planetary Change*, *41*(3-4), 207–214. https://doi.org/10.1016/j.gloplacha.2004.01.006

Lu, Y., Bookman, R., Waldmann, N., & Marco, S. (2020). A 45 kyr laminae record from the Dead Sea: Implications for basin erosion and floods recurrence. *Quaternary Science Reviews*, *229*, 106,143. https://doi.org/10.1016/j.quascirev.2019.106143

Lu, Y., Fang, X., Appel, E., Wang, J., Herb, C., Han, W., et al. (2015). A 7.3-1.6 Ma grain size record of interaction between anticline uplift and climate change in the western Qaidam Basin, NE Tibetan Plateau. *Sedimentary Geology*, *319*, 40–51. https://doi.org/10.1016/j.sedgeo.2015.01.008

Lu, Y., Fang, X., Friedrich, O., & Song, C. (2018). Characteristic grain-size component—A useful process-related parameter for grain-size analysis of lacustrine clastics? *Quaternary International*, *479*, 90–99. https://doi.org/10.1016/j.quaint.2017.07.027

Luo, Z., Su, Q., Wang, Z., Heermance, R. V., Garzione, C., Li, M., et al. (2018). Orbital forcing of Plio-Pleistocene climate variation in a Qaidam Basin lake based on paleomagnetic and evaporite mineralogic analysis. *Palaeogeography, Palaeoclimatology, Palaeoecology*, *510*, 31–39. https://doi.org/10.1016/j.palaeo.2017.09.022

Maslin, M., Li, X., Loutre, M.-F., & Berger, A. (1998). The contribution of orbital forcing to the progressive intensification of Northern Hemisphere glaciation. *Quaternary Science Reviews*, *17*(4–5), 411–426.

Mischke, S., Herzschuh, U., Zhang, C., Bloemendal, J., & Riedel, F. (2005). A Late Quaternary lake record from the Qilian Mountains (NW China): Lake level and salinity changes inferred from sediment properties and ostracod assemblages. *Global and Planetary Change*, *46*, 337–359. https://doi.org/10.1016/j.gloplacha.2004.09.023

Molnar, P. (2001). Climate change, flooding in arid environments, and erosion rates. *Geology*, *29*(12), 1071–1074.

Molnar, P., Anderson, R. S., Kier, G., & Rose, J. (2006). Relationships among probability distributions of stream discharges in floods, climate, bed load transport, and river incision. *Journal of Geophysical Research*, *111*, F02001. https://doi.org/10.1029/2005JF000310

Naafs, B. D. A., Hefter, J., Acton, G., Haug, G. H., Martínez-Garcia, A., Pancost, R., & Stein, R. (2012). Strengthening of North American dust sources during the late Pliocene (2.7Ma). *Earth and Planetary Science Letters*, *317-318*, 8–19. https://doi.org/10.1016/j.epsl.2011.11.026

Nagashima, K., Tada, R., Tani, A., Sun, Y., Isozaki, Y., Toyoda, S., & Hasegawa, H. (2011). Millennial-scale oscillations of the westerly jet path during the last glacial period. *Journal of Asian Earth Sciences*, *40*(6), 1214–1220. https://doi.org/10.1016/j.jseaes.2010.08.010

Nie, J., Garzione, C., Su, Q., Liu, Q., Zhang, R., Heslop, D., et al. (2017). Dominant 100,000-year precipitation cyclicity in a late Miocene lake from northeast Tibet. *Science advances*, *3*(3), e1600762. https://doi.10.1126/sciadv.1600762

Pross, J., & Klotz, S. (2002). Palaeotemperature calculations from the Praetiglian/Tiglian (Plio-Pleistocene) pollen record of Lieth, northern Germany: Implications for the climatic evolution of NW Europe. *Global and Planetary Change*, *34*(3–4), 253–267.

Pullen, A., Kapp, P., McCallister, A. T., Chang, H., Gehrels, G. E., Garzione, C. N., et al. (2011). Qaidam Basin and northern Tibetan Plateau as dust sources for the Chinese Loess Plateau and paleoclimatic implications. *Geology*, *39*(11), 1031–1034. https://doi.org/10.1130/g32296.1

Qiang, M., Chen, F., Zhang, J., Zu, R., Jin, M., Zhou, A., & Xiao, S. (2006). Grain size in sediments from Lake Sugan: A possible linkage to dust storm events at the northern margin of the Qinghai-Tibetan Plateau. *Environmental Geology*, *51*(7), 1229–1238. https://doi.org/10.1007/s00254-006-0416-9

Qiang, M., Chen, F., Zhou, A., Xiao, S., Zhang, J., & Wang, Z. (2007). Impacts of wind velocity on sand and dust deposition during dust storm as inferred from a series of observations in the northeastern Qinghai-Tibetan Plateau, China. *Powder Technology*, *175*(2), 82–89. https://doi.org/10.1016/j.powtec.2006.12.020

Qiang, M., Liu, Y., Jin, Y., Song, L., Huang, X., & Chen, F. (2014). Holocene record of eolian activity from Genggahai Lake, northeastern Qinghai-Tibetan Plateau, China. *Geophysical Research Letters*, *41*, 589–595. https://doi.org/10.1002/2013gl058806

Ravelo, A. C., Andreasen, D. H., Lyle, M., Lyle, A. O., & Wara, M. W. (2004). Regional climate shifts caused by gradual global cooling in the Pliocene epoch. *Nature*, *429*(6989), 263–267. https://doi.org/10.1038/nature02567

Raymo, M. E., & Ruddiman, W. F. (1992). Tectonic forcing of late Cenozoic climate. *Nature*, *359*(6391), 117–122.

Rea, D. K., Snoeckx, H., & Joseph, L. H. (1998). Late Cenozoic eolian deposition in the North Pacific: Asian drying, Tibetan uplift, and cooling of the Northern Hemisphere. *Paleoceanography*, *13*(3), 215–224.

Ruddiman, W. F., & Kutzbach, J. (1989). Forcing of late Cenozoic Northern Hemisphere climate by plateau uplift in southern Asia and the American West. *Journal of Geophysical Research*, *94*(D15), 18,409–18,427.

Schiemann, R., Lüthi, D., & Schär, C. (2009). Seasonality and interannual variability of the westerly jet in the Tibetan Plateau region. *Journal of Climate*, *22*(11), 2940–2957.

Shackleton, N. J., Backman, J., Zimmerman, H., Kent, D. V., Hall, M. A., Roberts, D. G., et al. (1984). Oxygen isotope calibration of the onset of ice-rafting and history of glaciation in the North Atlantic region. *Nature*, *307*(5952), 620–623. https://doi.org/10.1038/307620a0

Shang, Y., Kaakinen, A., Beets, C. J., & Prins, M. A. (2018). Aeolian silt transport processes as fingerprinted by dynamic image analysis of the grain size and shape characteristics of Chinese loess and red clay deposits. *Sedimentary Geology*, *375*, 36–48. https://doi.org/10.1016/j.sedgeo.2017.12.001

Shin, S., Liu, Z., Otto-Bliesner, B., Brady, E., Kutzbach, J., & Harrison, S. (2003). A simulation of the Last Glacial Maximum climate using the NCAR-CCSM. *Climate Dynamics*, *20*(2–3), 127–151.

Sosdian, S., & Rosenthal, Y. (2009). Deep-sea temperature and ice volume changes across the Pliocene-Pleistocene climate transitions. *Science*, *325*(5938), 306–310. https://doi.org/10.1126/science.1169938

Su, Q., Nie, J., Luo, Z., Li, M., Heermance, R., & Garzione, C. (2019). Detection of strong precession cycles from the late Pliocene sedimentary Records of Northeastern Tibetan Plateau. *Geochemistry, Geophysics, Geosystems*, *20*, 3901–3912. https://doi.org/10.1029/2019GC008447

Su, Q., Nie, J., Meng, Q., Heermance, R., Gong, L., Luo, Z., et al. (2019). Central Asian drying at 3.3 Ma linked to tropical forcing? *Geophysical Research Letters*, *46*, 10561–10567. https://doi.org/10.1029/2019GL084648

Sun, D., Bloemendal, J., Rea, D. K., An, Z., Vandenberghe, J., Lu, H., et al. (2004). Bimodal grain-size distribution of Chinese loess, and its palaeoclimatic implications. *Catena*, *55*(3), 325–340. https://doi.org/10.1016/s0341-8162(03)00109-7

Sun, Y., & An, Z. (2004). An improved comparison of Chinese loess with deep-sea $\delta^{18}O$ record over the interval 1.6–2.6 Ma. *Geophysical Research Letters*, *31*, L13210. https://doi.org/10.1029/2004gl019716

Sun, Y., An, Z., Clemens, S. C., Bloemendal, J., & Vandenberghe, J. (2010). Seven million years of wind and precipitation variability on the Chinese loess Plateau. *Earth and Planetary Science Letters*, *297*(3–4), 525–535. https://doi.org/10.1016/j.epsl.2010.07.004

Sun, Y., Clemens, S. C., An, Z., & Yu, Z. (2006). Astronomical timescale and palaeoclimatic implication of stacked 3.6-Myr monsoon records from the Chinese Loess Plateau. *Quaternary Science Reviews*, *25*, 33–48. https://doi.org/10.1016/j.quascirev.2005.07.005

Sun, Y., Clemens, S. C., Morrill, C., Lin, X., Wang, X., & An, Z. (2011). Influence of Atlantic meridional overturning circulation on the East Asian winter monsoon. *Nature Geoscience*, *5*(1), 46–49. https://doi.org/10.1038/ngeo1326

Talbot, M. R., & Allen, P. A. (1996). *Sedimentary environments: Processes, facies and stratigraphy*, 83–124 Ppp. Oxford: Blackwell Science Ltd.

Thompson, L. G., Mosley-Thompson, E., Davis, M., Lin, P., Dai, J., Bolzan, J., & Yao, T. (1995). A 1000 year climate ice-core record from the Guliya ice cap, China: Its relationship to global climate variability. *Annals of Glaciology*, *21*, 175–181.

Toggweiler, J. R., & Russell, J. (2008). Ocean circulation in a warming climate. *Nature*, *451*(7176), 286–288. https://doi.org/10.1038/nature06590

Vandenberghe, J., Zhisheng, A., Nugteren, G., Huayu, L., & Van Huissteden, K. (1997). New absolute time scale for the Quaternary climate in the Chinese loess region by grain-size analysis. *Geology*, *25*(1), 35–38.

Wang, J., Fang, X., Appel, E., & Song, C. (2012). Pliocene-Pleistocene climate change at the NE Tibetan Plateau deduced from lithofacies variation in the drill Core SG-1, western Qaidam Basin, China. *Journal of Sedimentary Research*, *82*(12), 933–952. https://doi.org/10.2110/jsr.2012.76

Wang, X., Yi, S., Lu, H., Vandenberghe, J., & Han, Z. (2015). Aeolian process and climatic changes in loess records from the northeastern Tibetan Plateau: Response to global temperature forcing since 30 ka. *Paleoceanography*, *30*, 612–620. https://doi.org/10.1002/2014pa002731

Williams, D., Peck, J., Karabanov, E., Prokopenko, A., Kravchinsky, V., King, J., & Kuzmin, M. (1997). Lake Baikal record of continental climate response to orbital insolation during the past 5 million years. *Science*, *278*(5340), 1114–1117.

Williams, G. P., & Bryan, K. (2006). Ice age winds: An aquaplanet model. *Journal of Climate*, *19*(9), 1706–1715.

Wischnewski, J., Mischke, S., Wang, Y., & Herzschuh, U. (2011). Reconstructing climate variability on the northeastern Tibetan Plateau since the last Lateglacial—A multi-proxy, dual-site approach comparing terrestrial and aquatic signals. *Quaternary Science Reviews*, *30*(1–2), 82–97. https://doi.org/10.1016/j.quascirev.2010.10.001

Xia, W., Zhang, N., Yuan, X., Fan, L., & Zhang, B. (2001). Cenozoic Qaidam basin, China: A stronger tectonic inversed, extensional rifted basin. *AAPG Bulletin*, *85*(4), 715–736.

Yang, B., Bräuning, A., Zhang, Z., Dong, Z., & Esper, J. (2007). Dust storm frequency and its relation to climate changes in Northern China during the past 1000 years. *Atmospheric Environment*, *41*(40), 9288–9299.

Yang, Y., Yang, R., Li, X., Han, W., Zan, J., Fang, X., et al. (2017). Glacial-interglacial climate change on the northeastern Tibetan Plateau over the last 600 kyr. *Palaeogeography, Palaeoclimatology, Palaeoecology*, *476*, 181–191. https://doi.org/10.1016/j.palaeo.2017.04.007

Yang, Z. L. (1986). Cenozoic lithofacies paleogeography and its evolution in Qaidam Basin. In Qinghai-institute-of-salt-lake (Ed.), *Evolution of Late Cenozoic geological environment in Qaidam Basin, Qinghai Province (in Chinese)*, (pp. 1–18). Beijing: Science Press.

Yao, T., Masson-Delmotte, V., Gao, J., Yu, W., Yang, X., Risi, C., et al. (2013). A review of climatic controls on $\delta^{18}O$ in precipitation over the Tibetan Plateau: Observations and simulations. *Reviews of Geophysics*, *51*, 525–548. https://doi.org/10.1002/rog.20023

Yin, A., Dang, Y. Q., Zhang, M., Chen, X. H., & McRivette, M. W. (2008). Cenozoic tectonic evolution of the Qaidam basin and its surrounding regions (part 3): Structural geology, sedimentation, and regional tectonic reconstruction. *Geological Society of America Bulletin*, *120*(7–8), 847–876. https://doi.org/10.1130/b26232.1

Zachos, J. C., Dickens, G. R., & Zeebe, R. E. (2008). An early Cenozoic perspective on greenhouse warming and carbon-cycle dynamics. *Nature*, *451*(7176), 279–283. https://doi.org/10.1038/nature06588

Zhang, H., Lu, H., Stevens, T., Feng, H., Fu, Y., Geng, J., & Wang, H. (2019). Expansion of dust provenance and aridification of Asia since ~7.2 Ma revealed by detrital zircon U-Pb dating. *Geophysical Research Letters*, *45*, 13,437–13,448. https://doi.org/10.1029/2018GL079888

Zhang, Q., & Liu, Q. (2018). Changes in diffuse reflectance spectroscopy properties of hematite in sediments from the North Pacific Ocean and implications for eolian dust evolution history. *Earth and Planetary Physics*, *2*(4), 1–9. https://doi.org/10.26464/epp2018031

Zhang, W., Appel, E., Fang, X., Song, C., Setzer, F., Herb, C., & Yan, M. (2014). Magnetostratigraphy of drill-core SG-1b in the western Qaidam Basin (NE Tibetan Plateau) and tectonic implications. *Geophysical Journal International*, *197*(1), 90–118. https://doi.org/10.1093/gji/ggt439

Zhang, Y. G., Ji, J., Balsam, W., Liu, L., & Chen, J. (2009). Mid-Pliocene Asian monsoon intensification and the onset of Northern Hemisphere glaciation. *Geology*, *37*(7), 599–602.